Characterization of Stoichiometric LiNbO$_3$ Grown from Melts Containing K$_2$O

G. I. Malovichko[1], V. G. Grachev[1], E. P. Kokanyan[2], O. F. Schirmer[3], K. Betzler[3], B. Gather[4],
F. Jermann[3], S. Klauer[3], U. Schlarb[3], and M. Wöhlecke[3]

[1] Institute of Materials Sciences, Ukrainian Academy of Sciences, Kiev, Ukraine
[2] Institute of Physical Researches, Ashtarak, Armenia
[3] FB Physik, Universität Osnabrück, Postfach 4469, W-4500 Osnabrück, Fed. Rep. Germany (Fax: 49-541/969-2670)
[4] FB Biologie/Chemie, Universität Osnabrück, Postfach 4469, W-4500 Osnabrück, Fed. Rep. Germany

Abstract. The growth of LiNbO$_3$ single crystals from a melt with the Li/Nb ratio of 0.946, to which 6 wt.% K$_2$O has been added, leads to stoichiometric specimens, essentially free of potassium, with (50 ± 0.15) mol% Li$_2$O in the crystal. This is established by studying the composition dependence of the following properties: linewidths of the electron paramagnetic resonance (EPR) of Fe^{3+}, energy of the fundamental absorption edge, Raman linewidths of phonon modes, and dispersion of the optical birefringence. Comparison of the results with relevant calibration scales leads to the above composition. In all cases the Li$_2$O content was found to be closer to 50% than that of a LiNbO$_3$ crystal vapor-phase equilibrated to 49.9 mol% Li$_2$O. The photorefractive effect at light intensities $I \geq 10^7$ W/m^2 is suppressed in this stoichiometric material. The features of the ternary system K$_2$O–Li$_2$O–Nb$_2$O$_5$, which are possibly responsible for the unexpected growth of stoichiometric LiNbO$_3$ from the indicated melts, are discussed.

PACS: 77.80.−e, 76.30.Fc, 61.50.Cj, 78.20.Jq

Lithium niobate (LiNbO$_3$) crystals have a considerable deficit of lithium (Li) ions, even if grown from melts with a Li content, $x_m = $ [Li]/([Li] + [Nb]) [1], exceeding 50% [2]. A qualitative indication of deviations from the stoichiometric composition can be obtained from the linewidths of the EPR of Fe^{3+} [3]. Using this method it was noticed recently [4], that crystals grown from melts with the nearly congruent composition, $x_m = 48.6\%$, to which 6 wt.% K$_2$O had been added, led to unusually sharp Fe^{3+} electron paramagnetic resonances, pointing to a crystal composition close to stoichiometric. Also the widths of ^{93}Nb nuclear magnetic resonance transitions $(m_I = 1/2 \leftrightarrow m_I = -1/2)$ turned out to be very narrow and not to depend on the angle between magnetic field and the crystal c-axis. This indicates that the distribution of the electric field gradients at the Nb sites is smaller than in conventional LiNbO$_3$ crystals and that nonaxially oriented gradients, attributed to intrinsic defects, are absent.

Using X-ray fluorescence and atomic absorption it was surprisingly found [4] that potassium (K) practically does not enter the crystals.

Here we report on the further characterization of such crystals. Our central goal is the determination of the Li content, x_c, in the crystal. There are two classes of experiments which yield this information. The most straightforward one is the chemical or physical determination of the relative numbers of Li and Nb ions in the crystal. These methods meet with great difficulties [5], and only recently the first results obtained in such a way, employing ion chromatography, have been published [2]. With respect to a critical assessment of these measurements, see [6]. The second class of methods uses the fact that deviations from stoichiometry will lead to intrinsic defects (density n_{def}), the most important among them being Nb$_{\text{Li}}$ antisite defects. For a review see [7]. These lattice perturbations will modify many features of the host lattice in a way depending on n_{def}, such as the ferroelectric, vibrational and optical properties. On this basis a composition dependence of, e.g., the Curie temperature [8], the Raman linewidths [9, 10], birefringence, [11], second-harmonic generation phase-matching temperature [12], fundamental optical absorption [13], has been observed. In addition, the properties of extrinsic defects are influenced by the presence of intrinsic ones. The preparation of LiNbO$_3$ crystals with defined Li/Nb ratios, using vapor transport equilibration (VTE) in atmospheres with such Li/Nb values [14], has proven to be very useful in furnishing standards by which other methods can be calibrated.

Among the many possible methods to determine the composition of our samples here we choose the following measurements: linewidths of the EPR of the background extrinsic defect Fe^{3+}, energy of the fundamental absorption edge, Raman linewidths of phonon modes, and dispersion of the optical birefringence. All four procedures identify the LiNbO$_3$ crystals to have a composition somewhat closer to stoichiometric than that of a VTE sample with $x_c = 49.9\%$.

From the absence of intrinsic defects in stoichiometric LiNbO$_3$ one expects an increased photo- and dark-conductivity of the material; thus the photorefractive effect should be reduced in these specimens. This has indeed been

found and will be reported here. In the following we shall first give information on the crystals studied and their preparation. Then we shall describe, in separate sections, the used methods of characterization and the results obtained. In the final part the results will be discussed. It will contain some remarks on the possible reasons why the addition of potassium to the melt can lead to stoichiometric material.

1 Experiments and Results

1.1 Crystals

Mainly three types of specimens were studied. They had been grown [4] using the Czochralski method from melts with the following compositions: $x_m = 48.6\%$ (nearly congruent), $x_m = 54.5\%$ and $x_m = 48.6\%$ with 6 wt.% K_2O (corresponding to 10.9 mol%) added to the melt. The first two specimens will be designated by the x_m of the melt from which they had been grown, and thus are called LN 48.6 and LN 54.5, respectively. The corresponding Li content in the crystal was found to be x_c(LN 48.6) = 48.6% and x_c(LN 54.5) = 49.5%, using birefringence and Raman measurements described in [10]. In all figures the Li content in the solid x_c is used. The crystal with 6 wt.% K_2O in the melt will be labelled LN 6 K. Since previous [93]Nb NMR, Fe^{3+} EPR [4] and optical absorption studies have shown that a behavior corresponding to ideally structured crystals is only obtained for K_2O not less than 6 wt.%, we shall list only potassium related results obtained with crystal LN 6 K. The potassium content of these specimens was determined with an electron microprobe to be 0.022 ± 0.004 wt.%. The error range represents the limit of potassium detectivity. This newly determined potassium concentration is in accord with that found previously [4] using different methods: $[K] \lesssim 10^{-2}$ wt.%.

The VTE crystal used for comparison was purchased from Crystal Technology, Palo Alto, CA. Its x_c had been determined to be 49.9% [6]. This specimen will be labelled LN VTE in the following.

1.2 EPR of Fe^{3+}

All $LiNbO_3$ crystals, even if grown from rather pure melts, contain Fe as a trace impurity. The unintended Fe^{3+} ($3d^5$, $S = 5/2$) content of the specimens investigated here is used to probe the crystal quality. The corresponding EPR lines of crystal LN 6 K (Fig. 1). are narrower than those of Fe^{3+} in any other $LiNbO_3$ material previously studied, irrespective of its origin, treatment or compositon. The characteristics of the EPR spectra (width, intensity, shape of lines) depend on the crystal fields at the Fe^{3+} sites, which in turn are influenced by the composition. In the ideal $LiNbO_3$ structure all cation sites have C_3 symmetry, and the spin-Hamiltonian of centers with $S = 5/2$ consists of the operators ([3], for notation see [15])

$$\mathcal{H} = \beta \mathbf{B} \mathbf{g} \mathbf{S} + b_2^0 O_2^0 + b_4^0 O_4^0 + b_4^3 O_4^3 \tag{1}$$

The spectrum at $B \| c$, calculated with this spin-Hamiltonian contains only "allowed" transitions, corresponding to a change of the electron spin quantum number $\delta M_s + \pm 1$,
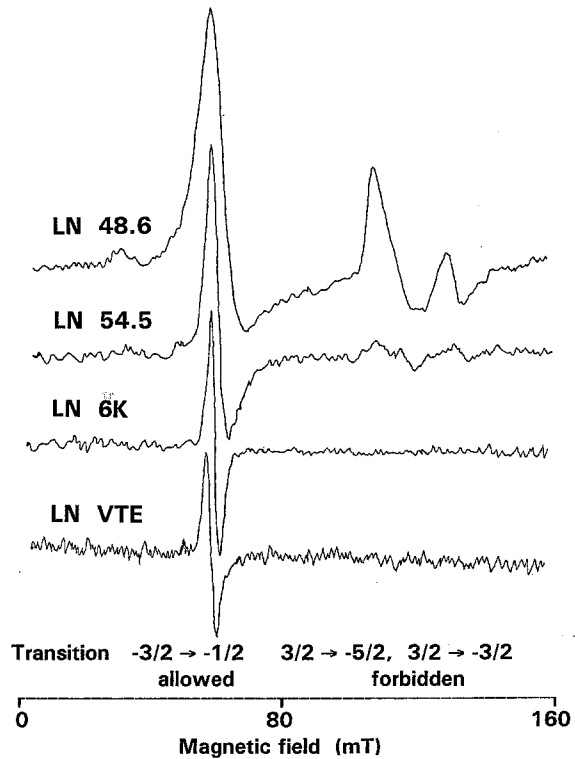
Fig. 1. Low field EPR lines of Fe^{3+} in $LiNbO_3$ crystals of various compositions for $B \| c$ and microwave frequency $\nu = 9.018$ GHz at room temperature

and "forbidden" ones with $\delta M_s = \pm 2, \pm 3, \ldots$ are absent. In real crystals, especially those with a composition far from stoichiometric, some randomly distributed intrinsic defects can be located near to a paramagnetic ion, such as Fe^{3+}. These defects distort the crystal fields at the site of the ion and reduce its point symmetry from C_3 to C_1. Therefore, the following term should be added to (1):

$$\mathcal{H}_{\text{def}} = \sum_{k=2,4} \sum_{q=1,2,4} (b_k^q \Omega_k^q + c_k^q \Omega_k^q). \tag{2}$$

It should be pointed out that the values of b_k^q and c_k^q can differ considerably from one center to another and that their mean values will grow with increasing defect concentration n_{def}. The decrease of the symmetry of the center leads to the following observable features of the spectra.

1. Forbidden transitions with $\delta M_s = \pm 2, \pm 3, \ldots$ arise at $B \| c$. These include the following: $M_s = -3/2 \leftrightarrow M_s = 1/2, -3/2 \leftrightarrow 3/2, -5/2 \leftrightarrow 1/2$ and $-5/2 \leftrightarrow 3/2$. Their intensities are proportional to the ratio of the matrix element squares of $\mathcal{H}_{\text{def}}$ and $\mathcal{H}$ and, of course, will rise with the increase of n_{def}.

2. An asymmetry of the lineshapes of the allowed transitions (such as the $-3/2 \leftrightarrow -1/2$ line (Fig. 1) and the central $1/2 \leftrightarrow -1/2$ transition) can appear at $B \| c$. Low-symmetry components of crystal fields change the calculated position of these lines only in second-order perturbation theory. The existence of random square shifts causes the line asymmetry [3].

3. The widths of the lines may become angular dependent with rising n_{def}. If the angle between B and c increases, $\mathcal{H}_{\text{def}}$ leads to first order line shifts and this effect is usually

greater than the second-order one. For crystals with high n_{def} the linewidths then become angular dependent. The widths and the amplitudes of their angular changes depend on n_{def}.

In Fig. 1 the Fe^{3+} lines occurring at the lowest magnetic fields in the above mentioned crystals are shown. It is seen, that in the VTE and LN 6 K crystals only the allowed transition takes place, having a very narrow width and symmetrical shape. The intensities of the forbidden lines, though weak, are still nonzero in LN 54.5. This indicates that these crystals, although grown from a melt with a high Li surplus, are far from ideal. Finally, crystals with a nearly congruent composition, LN 48.6, have such high concentrations of symmetry lowering defects that the forbidden lines are equally intense as the allowed ones.

This argument can be put on a more quantitative basis if the widths of the two lowest allowed transitions for $B\perp c$ at 295 K and 14 K are plotted (Fig. 2) as a function of x_c. The widths of these lines are more sensitive to n_{def} than those at $B\|c$ (see item 3 of this section). It is observed in Fig. 2 that the widths of the lines of LN 6 K (horizontally dotted) are somewhat narrower than those of the VTE crystal, the latter corresponding to the calibration point at $x_c = 49.9\%$. LN 6 K thus has the tendency to have a composition somewhat closer to stoichiometric than the VTE crystal.

The plot in Fig. 2 furthermore shows that the linewidths of the EPR of Fe^{3+} can also be used to determine x_c quantitatively. By extrapolating the x_c data obtained with the nearly congruent crystal, LN 48.6, with LN 54.5 [3] and with the VTE material at both 295 K and 14 K we find x_c of LN 6 K to be 49.95 ± 0.10.

It was also observed that the linewidths of all transitions have no angular dependence in LN 6 K (except, of course, the ranges of angles, for which resonance transitions take place near the crossing of energy levels).

1.3 Fundamental Optical Absorption

The position of the fundamental absorption edge of LiNbO₃ is a sensitive indicator for the Li/Nb composition of the
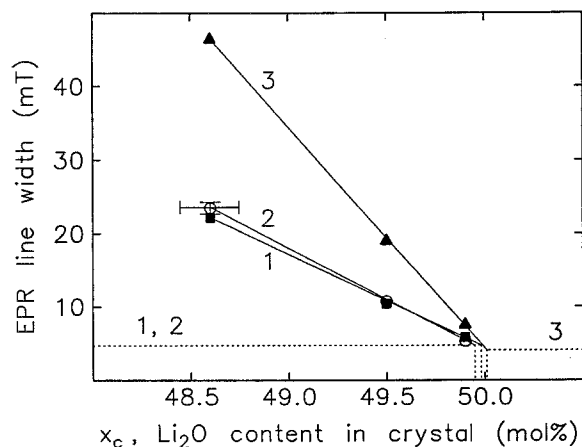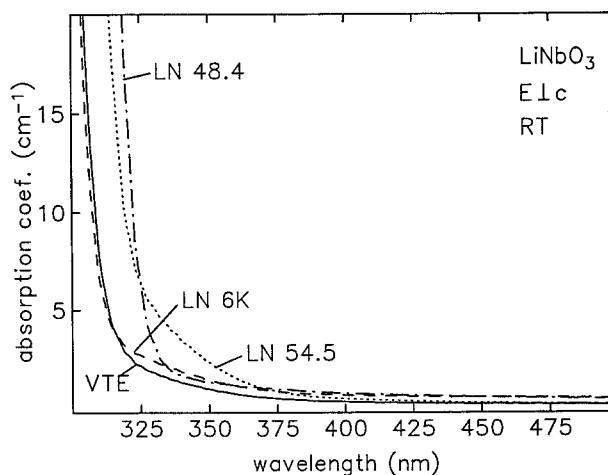
Fig. 3. Optical absorptions, near the fundamental edge, corrected for reflection, of the nearly stoichiometric crystals, LN 6 K and LN VTE, and of crystals LN 48.6 and LN 54.5

material [13]. A pronounced blue shift occurs if the Li content rises. For congruent material, e.g., Földvari et al. [13] have found the edge to lie at 320 nm and for a sample grown from a stoichiometric melt ($x_m = 50\%$) at 318 nm. Here we define the position of the edge as the wavelength, where the absorption coefficient is $15\,cm^{-1}$ at 295 K.

The results of our absorption measurements are shown in Fig. 3. For LN 48.6, the edge again is found at 320 nm and for LN 54.5 at 317 nm. There is a huge further shift to 306 nm and 305 nm for the LN VTE and the LN 6 K samples, respectively. The near coincidence of the edges for both materials indicates that also LN 6 K has a composition close to stoichiometric with LN 6 K somewhat closer to $x_c = 50\%$. It should be noted that LN 6 K shows an additional absorption for $\lambda > 320\,nm$ extending up to 700 nm. The origin of this optical density is not known yet. It is about twice as strong for $E\|c$ than for $E\perp c$, the latter being shown in Fig. 3.

1.4 Raman Linewidths of Phonon Modes

Raman scattering was among the first methods to characterize the stoichiometry of LiNbO₃ [9]. The underlying effect is a homogeneous and an inhomogeneous broadening of phonon linewidths. The temperature-dependent homogeneous broadening is mainly due to anharmonicities of the interionic potentials, while the inhomogeneous contributions are caused by irregularities of the translational and site symmetry of the lattice. Thus compositional changes, especially deviations from stoichiometry, are reflected in the inhomogeneous part. Temperature dependent determinations of the half widths have shown, that the inhomogeneous part is a temperature-independent constant contribution to the total linewidth [10]. Therefore, comparative studies have to be carried out at a constant temperature. For reasons of convenience we used conventional right-angle-scattering geometries at room temperature.

For an unambiguous determination of the linewidth Γ (full width at half maximum) we have chosen the E and

Fig. 2. Dependence of Fe^{3+} EPR linewidths on Li₂O content, x_c, for $B\perp c$. 1,2: transitons at 60 mT and 130 mT, $\nu = 9.018\,GHz$, room temperature; 3: transition at 300 mT, $\nu = 9.051\,GHz$, $T = 14\,K$. The horizontal dotted lines corresond to the linewidths of the crystal LN 6 K
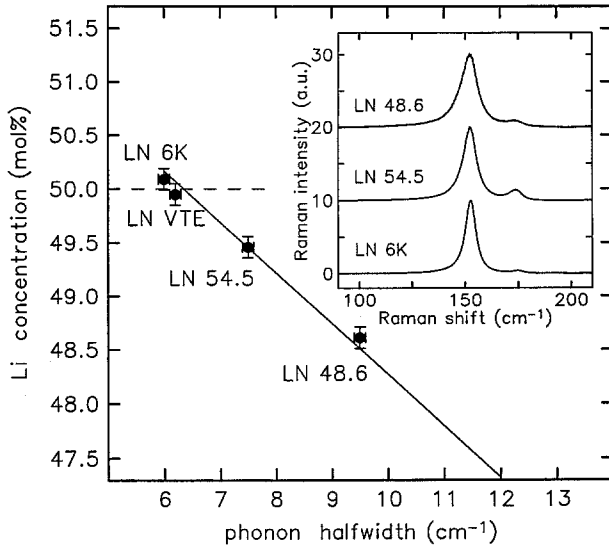
Fig. 4. Li concentration x_c plotted vs the half width Γ of the E phonon at 153 cm^{-1} for the four crystals discussed in the text (filled dots) determined from the Raman spectra in the inset. The straight line represents the linear relation (3) determined in [10]. Inset: Raman lineshape of the E phonon at 153 cm^{-1} for the three crystals LN 48.6, LN 54.5, LN 6 K from top to bottom

A_1 modes at 153 cm^{-1} and 876 cm^{-1}, measurable in the configurations $Z(YZ)X$ and $Z(YY)X$, respectively. These lattice vibrations show only weak directional dispersion and their bands do not overlap with other bands.

In contrast to the work of Balanevskaya et al. [9], where Γ was related to the composition of the melt, we used the dependence of Γ on the composition of single crystals [10]. A linear relation results for each mode, e.g.,

$$x_c \,[\text{mol}\%] = 53.03 - 0.4739 \Gamma \,[\text{cm}^{-1}] \qquad (3)$$

for the 153 cm^{-1} phonon and

$$x_c \,[\text{mol}\%] = 53.29 - 0.1837 \Gamma \,[\text{cm}^{-1}] \qquad (4)$$

for the 876 cm^{-1} phonon. The concentration is to be given in mol% and Γ in wavenumbers.

In the inset of Fig. 4 we show the spectra of the E phonon at 153 cm^{-1} recorded with the three crystals discussed here. The half width decreased when going from the LN 48.6 sample to the LN 54.5 and LN 6 K. The same result is also found for the A_1 phonon at 876 cm^{-1}. The linewidths Γ determined from the spectra for the samples LN 48.6, LN 54.5, LN VTE, and LN 6 K are 9.5, 7.5, 6.2, and 6.0 cm^{-1} for the 153 cm^{-1} phonon and 23.7, 21.0, 18.1, and 18.0 cm^{-1} for the 876 cm^{-1} phonon, respectively, with an uncertainty $\Delta\Gamma \approx 0.1$ cm^{-1} in all cases. The Li concentration x_c can be calculated from these values using (3) and (4) for both phonons. Within the experimental error the evaluation of both phonon linewidths leads to a similar Li concentration. The averaged x_c values calculated from (3) and (4) are plotted against the linewidth Γ of the 153 cm^{-1} phonon for all four samples in Fig. 4. The straight line represents the linear correlation implied by (3). Within the experimental uncertainty for Γ the band shape of the K_2O grown crystal resembles that of the VTE crystal, although for both phonons the linewidths of LN 6 K are slightly lower than those of

LN VTE. This indicates, similar to the results of the other methods, that x_c of the LN 6 K crystal is slightly above that of LN VTE.

1.5 Dispersion of Birefringence

In order to determine x_c in LN 6 K quantitatively its birefringence was compared, using a new highly accurate interferometric method [16], with that of the mentioned LN VTE. In contrast to the investigation of second-harmonic generation, where the matching of n_e and n_o at only two frequencies is determined, the present method offers the opportunity to check the coincidence between probe and reference samples over a wide spectral range with high accuracy. This allows also to detect spectral anomalies, here possibly arising from the used growth method, involving potassium in the melt. Figure 5 shows the results obtained with crystal LN 6 K (full dots) as compared to LN VTE (open circles) and crystal LN 54.5 (triangle). It is seen that there is excellent coincidence between the data of both the VTE crystal and of LN 6 K, indicating a comparable composition of both specimens. The lines in Fig. 5 are based on a generalized two-term Sellmeier fit [17], which excellently describes the refractive indices for all known compositions of LiNbO$_3$ over a wide spectral range. A least square fit aproach again yields 50.0 ± 0.1% Li content for LN 6 K. It is seen that x_c in LN 54.5 is only 49.5%, as already mentioned in the experimental part. The measured dispersion of $n_e - n_o$ of specimen LN 6 K does not show any deviation from the expected behavior. Thus a possible contribution of potassium to the birefringence cannot be identified. This may be attributed to the low potassium content in the crystal.

1.6 Photorefractive Properties

The light-induced changes of the birefringence $\delta(n_e - n_o)$ (abbreviated $\delta\Delta n$ in the following) of congruent and stoichiometric crystals have been measured at light intensities between 10^5 and 10^8 W/m^2. Utilizing a focussed, extraordinary polarized Ar$^+$-ion laser beam ($\lambda_{Ar} = 514.5$ nm) with
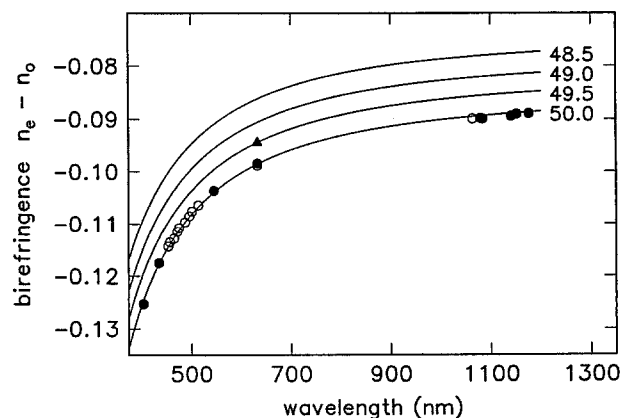
Fig. 5. Dispersion of the optical birefringence of the following LiNbO$_3$ crystals: LN 6 K (full dots), LN VTE (open circles) and LN 54.5 (triangle). The full lines represent the calculated birefringences for LiNbO$_3$ with the indicated Li contents

a Gaussian width δw of $28 \pm 3\,\mu$m to induce the changes, we determined $\delta \Delta n$ by the optical phase-compensation technique [18] using a co-axial, narrow ($\delta w = 13\pm2\,\mu$m) HeNe-laser beam ($\lambda_{\text{HeNe}} = 632.8$ nm). The experimental setup was checked by remeasuring $\delta \Delta n$ of a congruent sample, which had been characterized previously in another laboratory [19]. Within the accuracy of our measurements, about $\pm15\%$ relative error of $\delta \Delta n$ and $\pm40\%$ of light intensity, both results are identical.

Figure 6 exhibits the dependences of $\delta \Delta n$ on light intensity for stoichiometric LiNbO₃, LN 6K, as well as for a congruent sample. It is seen that the saturation values of $\delta \Delta n$ depend strongly on intensity. The patterns of the dependences, however, are clearly different. The index change $\delta \Delta n$ of congruent LiNbO₃ increases rapidly with rising intensity and does not show a tendency to saturation. For the stoichiometric crystal, on the other hand, $\delta \Delta n$ is comparatively high at the weak intensities and becomes independent at strong ones. Most important, it is found that the maximum index change of the stoichiometric sample is about 5 times lower at high intensities ($I \approx 3 \times 10^7$ W/m²) than in congruent LiNbO₃, indicating that the optical damage is suppressed in stoichiometric material at high intensities.

In order to compare our results with those of holographic measurements, where the light induced change of only one refractive index, say δn_e, is determined instead of $\delta \Delta n$, we relate these two quantities to each other, using

$$\delta n_e = \delta \Delta n / (1 - n_o^3 r_o / n_e^3 r_e),$$

where δn_e and $\delta \Delta n$ are the respective maximum saturation values at a given intensity, and r_o, r_e are the Pockels coefficients [19] relevant in the present experiment. For the present stoichiometric crystal both holographic and compensator measurements have been performed. They yield $n_e^3 r_e / n_o^3 r_o = 2.80 \pm 0.08$. This is in very good agreement with the value 2.83 ± 0.06 calculated from the refractive indices measured for stoichiometric LiNbO₃ [17] and the ratio of the electro-optic coefficients determined in [20] for congruent crystals. The latter ratio thus appears to be independent of crystal composition.
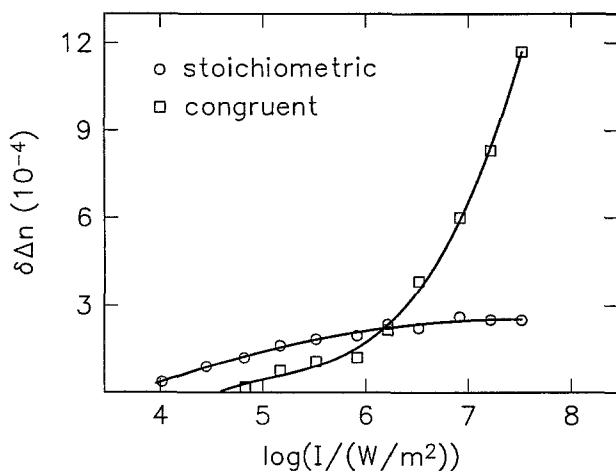
Another remarkable result is that, for the stoichiometric crystal, we failed to find an intensity region in which the saturation value δn_e clearly does not depend on light intensity. Additional holographic measurements with intensities less than 1 kW/m² verify this, in contradiction to all results with congruent crystals [19, 21].

2 Discussion

The various methods used to determine the composition of LN 6K have shown in all cases that x_c of this specimen is closer to 50% than that of the VTE crystal compared. Quantitatively it was found that $x_c = (50.00 \pm 0.15)\%$, where the error range has been pessimistically chosen to encompass the results of all separate determinations. These results mean that a convenient method has been identified by which stoichiometric LiNbO₃ can be produced. So far it is the only way to obtain bulk-stoichiometric material. Because of the rather slow ion transport in LiNbO₃, necessitating at least 60 h of vapor phase equilibration treatment at 1100° C to obtain stoichiometric LiNbO₃ of 0.5 mm thickness [6], the VTE procedure is limited practically to the preparation of material at most 3 mm thick. In contrast to the present method the delicate VTE process has to be performed in addition to the crystal growth. As shown once more in the present paper, the growth of LiNbO₃ from binary melts with a considerable Li surplus does not produce stoichiometric material, in contrast to many publications stating opposite views.

The question arises why the addition of potassium to the melt leads to stoichiometric LiNbO₃ crystals. Some hints can be obtained from the information about the ternary system K₂O–Li₂O–Nb₂O₅ available in the literature. The published phase diagrams [22, 23] show (Fig. 7) that in the solid phase
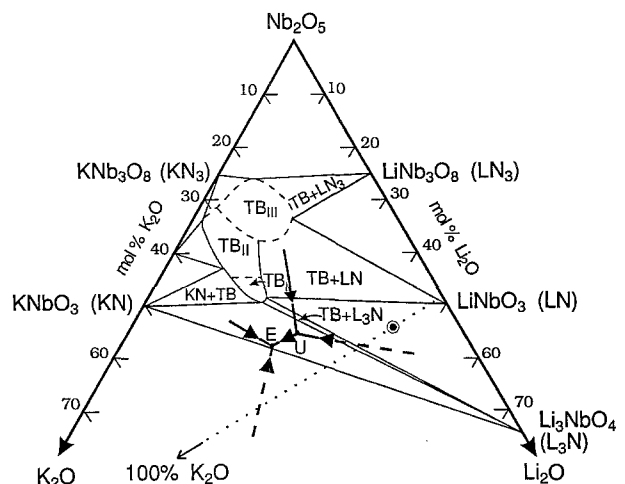
Fig. 7. Phase diagrams for the ternary system K₂O–Li₂O–Nb₂O₅. a) Thin lines: subsolidus (solid phase), adapted from [22]. The ball marks the composition of the melt of LN 6K. In the solid phase it lies in the triangle indicating the three-phase equilibrium with the corners LiNbO₃ (close to stoichiometric), Li₃NbO₄ and a phase with the tungsten-bronze-type structure (TB). b) The thick lines mark boundaries (adapted from [23]) on the liquidus surface, confining the relevant primary crystallization regions. The melt composition of LN 6K lies on the primary crystallization surface of LiNbO₃

Fig. 6. Intensity dependence of the saturation values of the light-induced birefringence changes for congruent and stoichiometric (LN 6K) LiNbO₃ crystals. The solid lines are guides to the eye

a three-phase equilibrium of $LiNbO_3$, Li_3NbO_4 and tungsten bronze type structure (with the composition 51% Nb_2O_5, 28.5% K_2O and 20.5% Li_2O) exists. The addition of 6 wt.% (10.9 mol%) K_2O to congruently melting $LiNbO_3$ leads to a composition lying in the indicated three-phase field, as marked in Fig. 7. Since the melting temperature is lowered by the addition of K_2O, the growth process is shifted towards the solid-state equilibrium conditions, where $LiNbO_3$ is one of the compounds at the corners of the three-phase triangle. So it is expected that $LiNbO_3$ grown from a melt with the indicated composition will be nearly stoichiometric.

That $LiNbO_3$ crystals can indeed be grown from such melts is indicated by the boundaries of the primary crystallization liquidus surface of $LiNbO_3$ [23], shown with thick lines in Fig. 7. It is seen that the melt composition of LN 6 K lies on this primary crystallization surface for K_2O concentrations up to about 15 mol%.

The described three-phase equilibrium in the solid phase is consistent only with a solidus surface steeply inclined along the K_2O direction of the phase diagram. Only this assumption is in line with the fact that no mixed phase with a measurable K_2O width has been identified (Fig. 7). On this basis it can be understood that at most 10^{-2} wt.% K is incorporated into the crystals.

The main effect of the K_2O admixture obviously consists in a dilution of the $LiNbO_3$ melt. In general, all appropriate fluxes or solutions tend to favour the growth of stoichiometric crystals. Dilution reduces effects which hamper the crystal formation activity of components of concentrated melts. In $LiNbO_3$ such an effect seems to be the dynamic formation of Li_3NbO_4 clusters in the melt. (Because of its high melting point, 1406° C, Li_3NbO_4 should be the thermodynamically most stable compound in the $Li_2O-Nb_2O_5$ system; the existence of such precrystalline clusters is furthermore indicated by the anomalous behavior of the viscosity of $LiNbO_3$ melts [24], occurring at 1270° C, somewhat below the melting point of Li_3NbO_4.) In concentrated melts the dynamic formation and re-solution of such clusters can reduce the effective Li concentration at the liquid–solid boundary, thus yielding Li defective crystals.

It is seen that the remarkable fact that stoichiometric, nearly potassium free $LiNbO_3$ crystals can be grown from the indicated melt is compatible with the available information on the ternary system $K_2O-Li_2O-Nb_2O_5$. Further investigations have to be performed in order to clarify all details of the growth process.

The availability of bulk-stoichiometric $LiNbO_3$ crystals opens a rich field for further investigations and applications. One may first think of more refined investigations of defects and their compensation processes. With respect to applications our results have shown that at least at high intensities the present crystals suppress optical damage. It remains to be investigated whether unwanted impurities, possibly connected to the additional optical absorption of LN 6 K (Fig. 3), can be removed and whether this will decrease the photorefractive index changes also at low intensities. One of the

main future objectives in this field should be, however, the definite identification of the crystal-growth mechanism responsible for the unexpected result. A clarification of this point should have an impact on the growth procedures of other crystalline materials.

References

1. In this paper mainly the quantity $x = [Li]/([Li] + [Nb])$ will be used to characterize melts or crystals. This x is equal to the Li_2O mole fraction. Alternatively the ratio $Li/Nb = R$ can be employed. Both systems are related to each other by $x = R/(1 + R)$ and $R = x/(1 - x)$. Subscripts m and c will be used to designate melt and crystal, respectively

2. B.C. Grabmaier, F. Otto: J. Crystal Growth **79**, 682 (1986)

3. G.I. Malovichko, V.G. Grachev, V.T. Gabrielyan, E.P. Kokanyan: Sov. Phys. – Sol. State **28**, 1453 (1986)

4. G.I. Malovichko, V.G. Grachev, L.P. Yurchenko, V.Y. Proshko, E.P. Kokanyan, V.T. Gabrielyan: Phys. Status Solidi (a) **133** (1992)

5. A. Räuber: In *Current Topics in Materials Science*, ed. by E. Kaldis, Vol. 1 (North-Holland, Amsterdam 1978) p. 48

6. D.H. Jundt, M.M. Feijer, R.L. Byer: IEEE J. QE-**26**, 135 (1990)

7. O.F. Schirmer, O. Thiemann, M. Wöhlecke: J. Phys. Chem. Solids **52**, 185 (1991)

8. J.R. Carruthers, G.E. Peterson, M. Grasso, P.M. Bridenbaugh: J. Appl. Phys. **42**, 1846 (1971)

9. A.E. Balanevskaya, L.I. Pyatigorskaya, Z.I. Shapiro, L.N. Margolin, E.A. Bovina: J. Appl. Spectrosc. **38**, 491 (1983)

10. U. Schlarb, S. Klauer, M. Wesselmann, K. Betzler, M. Wöhlecke: To be published

11. E. Born, E. Willibald, R. Veith: In *Proc. IEEE Ultrasonics Symposium*, ed. by B.R. McAvoy (IEEE, New York 1984) p. 268

12. N. Schmidt, K. Betzler, B.C. Grabmaier: Ferroelectrics Lett. **10**, 133 (1989)

13. I. Földvari, K. Polgár, R. Voszka, R.N. Balasanyang: Crystal Res. Technol. **19**, 1659 (1984)

14. P.F. Bordui, R.G. Norwood, D.H. Jundt, M.M. Feijer: J. Appl. Phys. **71**, 875 (1992)

15. S.A. Altshuler, B.M. Kozyrev: Electron Paramagnetic Resonance in Conpounds of Transition Elements (Wiley, New York 1974)

16. U. Schlarb, K. Betzler: Ferroelectrics **126**, 39 (1992)

17. U. Schlarb, K. Betzler: To be published

18. F.S. Chen: J. Appl. Phys. **40**, 3389 (1969)

19. O. Althoff, E. Krätzig: Nonlinear Optical Materials III, SPIE, Vol. 1273, 12 (1990)

20. S. Fries, S. Bauschulte: Phys. Status Solidi (a) **125**, 369 (1991)

21. E. Krätzig, R. Sommerfeld: Nonlinear Optical Materials III, SPIE, Vol. 1273, 2 (1990)

22. T. Ikeda, K. Kiyohashi: Jpn. J. Appl. Phys. **9**, 12 (1979)

23. B.A. Scott, E.A. Gies, B.L. Olson, G. Burns, A.W. Smith, D.F. O'Kane: Mater. Res. Bull. **5**, 50 (1970)

24. K. Shigematsu, Y. Anzai, S. Morita, M. Yamada, H. Yokoyama: Jpn. J. Appl. Phys. **26**, 1988 (1978)